Biochimica et Biophysica Acta 1817 (2012) 1196–1207

Contents lists available at SciVerse ScienceDirect

Biochimica et Biophysica Acta

journal homepage: www.elsevier.com/locate/bbabio

Fast structural changes (200–900 ns) may prepare the photosynthetic manganese complex for oxidation by the adjacent tyrosine radical ☆

André Klauss, Thomas Sikora, Björn Süss, Holger Dau *

Free University Berlin, Physics Department, 14195 Berlin, Germany

ARTICLE INFO

Article history:
Received 1 February 2012
Received in revised form 25 April 2012
Accepted 30 April 2012
Available online 8 May 2012

Keywords:
Optoacoustic
Oxygen evolution
Photoacoustic
Photosynthesis
Photosystem II
Water oxidation

ABSTRACT

The Mn complex of photosystem II (PSII) cycles through 4 semi-stable states (S_0 to S_3). Laser-flash excitation of PSII in the S_2 or S_3 state induces processes with time constants around 350 ns, which have been assigned previously to energetic relaxation of the oxidized tyrosine (Y_Z^{ox}). Herein we report monitoring of these processes in the time domain of hundreds of nanoseconds by photoacoustic (or 'optoacoustic') experiments involving pressure-wave detection after excitation of PSII membrane particles by ns-laser flashes. We find that specifically for excitation of PSII in the S_2 state, nuclear rearrangements are induced which amount to a contraction of PSII by at least 30 $Å^3$ (time constant of 350 ns at 25 °C; activation energy of 285 +/− 50 meV). In the S_3 state, the 350-ns-contraction is about 5 times smaller whereas in S_0 and S_1, no volume changes are detectable in this time domain. It is proposed that the classical $S_2 => S_3$ transition of the Mn complex is a multi-step process. The first step after Y_Z^{ox} formation involves a fast nuclear rearrangement of the Mn complex and its protein–water environment (~350 ns), which may serve a dual role: (1) The Mn- complex entity is prepared for the subsequent proton removal and electron transfer by formation of an intermediate state of specific (but still unknown) atomic structure. (2) Formation of the structural intermediate is associated (necessarily) with energetic relaxation and thus stabilization of Y_Z^{ox} so that energy losses by charge recombination with the Q_A^- anion radical are minimized. The intermediate formed within about 350 ns after Y_Z^{ox} formation in the S_2-state is discussed in the context of two recent models of the $S_2 => S_3$ transition of the water oxidation cycle. This article is part of a Special Issue entitled: Photosynthesis Research for Sustainability: From Natural to Artificial.

1. Introduction

Photosynthesis of plants, algae and cyanobacteria is of undeniable importance for life on earth [1]. The light-driven water oxidation catalyzed by the protein-bound Mn_4Ca complex of photosystem II (PSII) [2,3] plays a pivotal role and is of high interest also as an inspiration or even blueprint for technological systems designed for production of solar fuels [4–8]. In the last years, stunning progress has been obtained with respect to resolving the structure of the catalytic site at the atomic level [9–13] (see Fig. 1) as discussed in full detail elsewhere [14]. A reaction cycle model has been proposed describing the basic sequence of electron and proton removal from the Mn complex [15,16,3]. (Here and in the following, the Mn complex—also denoted as oxygen-evolving complex (OEC)—is considered to include the $Mn_4Ca(\mu\text{-}O_5)$ core as well as its ligand environment, but not the redox-active tyrosine residue denoted as Y_Z.) Reaction cycle and mode of O–O bond formation have been addressed in computational studies [12,17,18]. In the present investigation, we will address another facet of photosynthetic water oxidation. We report evidence that fast nuclear rearrangements (about 400 ns at 20 °C) precede oxidation of the Mn complex thereby achieving stabilization of the charge-separated state and likely also preparation of the active site for the subsequent electron and proton transfer steps.

Absorption of one photon by the PSII antenna pigments is followed first by primary and secondary electron transfer resulting in formation of the $P680^+Q_A^-$ radical pair within less than 1 ns [19–21], where $P680^+$ refers to a specific oxidized chlorophyll (Chl) species and Q_A^- to the reduced primary quinone acceptor. More than 20 years ago, it was found that the reduction of $P680^+$ by Y_Z, the redox-active Tyr161 of the D1 subunit of PSII, exhibits a multiphasic time course in the nanosecond and microsecond time domain with a marked dependence on the oxidation state of the Mn_4Ca complex [22,23]. Fast nanosecond kinetics in the range of 20–60 ns were later interpreted [24] as monitoring electron transfer coupled to a proton shift within a hydrogen bond between Y_Z and the nearby His190 of the D1 polypeptide [25]. Slow nanosecond kinetics were found to be more pronounced for the OEC in its S_2 or S_3 state than for the OEC in the lower oxidation states, S_0 and S_1 [22,23,26–30] (S_0, S_1, S_2 and S_3 refer to the stable (S_1) or semi-stable oxidation state of the Mn complex; the subscript indicates the number

Abbreviations: chl, chlorophyll; ET, electron transfer; MES, 2-morpholinoethane-sulfonic acid; LIOAS, laser-induced optoacoustic spectroscopy; PA, photoacoustic; PSII, photosystem II

☆ This article is part of a Special Issue entitled: Photosynthesis Research for Sustainability: from Natural to Artificial.

* Corresponding author at: Freie Universität Berlin, Fachbereich Physik, Arnimallee 14, 14195 Berlin, Germany. Tel.: +49 30 838 53581; fax: +49 30 8385 6299.
E-mail address: holger.dau@fu-berlin.de (H. Dau).

0005-2728/$ – see front matter © 2012 Elsevier B.V. All rights reserved.
doi:10.1016/j.bbabio.2012.04.017

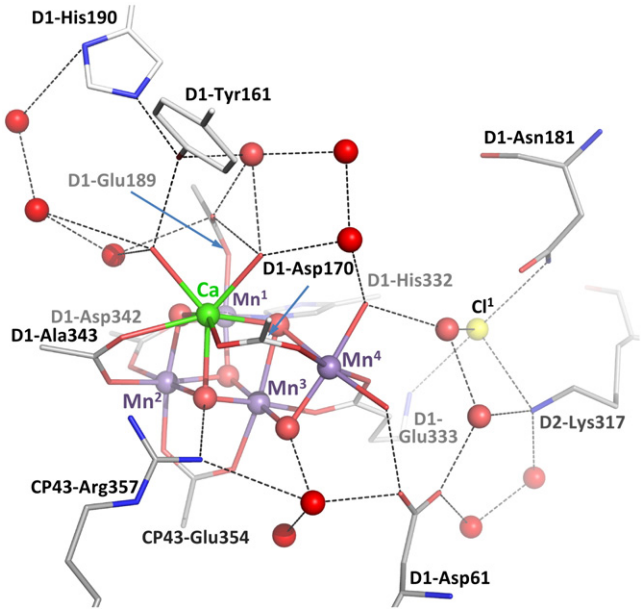

Fig. 1. Water-oxidizing manganese complex and redox-active tyrosine of photosystem II (PSII). The $Mn_4Ca(\mu\text{-}O)_5$ core of the Mn complex is bound to amino acid residues of the D1 and of the CP43 protein. Within about 50 ns after absorption of a light quantum by the antenna pigments of PSII, D1-Tyr161 (denoted as Tyr_Z or Y_Z) is oxidized by $P680^+$ (not shown), the primary electron donor. The oxidation of Y_Z most likely is coupled to a shift of the phenolic proton toward D1-His190. Consequently Y_Z^{ox} formally is a neutral radical ($Y_Z^{\bullet}$), but the $[Y_Z^{\bullet}\cdots H\text{-}NHis190]^+$ moiety is positively charged. (For simplicity, we will denote the $[Y_Z^{\bullet}\cdots H\text{-}NHis190]^+$ moiety as Y_Z^{+}.) The oxygen atoms of water molecules are depicted as red spheres; water-derived terminal ligands of Mn and Ca are indicated as red sticks. Putative hydrogen bonds are depicted as broken lines between the H-bond donor and acceptor (both mostly oxygens). Aside from the ligating residues, further polar residues as well as a chloride ion of functional importance are shown. The following color code was used: red, oxygen; purple, manganese; blue, nitrogen; green, calcium; yellow, chloride. (All atom coordinates from PDB entry 3ARC [13]).

of accumulated oxidation equivalents [31,32]). High activation energies and reorganization energies have been reported for the slow nanosecond components of $P680^+$ reduction in the S_2 and S_3 state [30]. It was assumed that relaxation processes lower the Gibbs energy of Y_Z^{OX} relative to $P680^+$ and thereby further stabilize the $P680Y_Z^{ox}$ state [27,33,24]. A significant kinetic isotope effect (KIE) upon H_2O/D_2O exchange was not detectable [34,27]. These results lead to the assumption that proton relocations are not rate limiting in this relaxation process [24]. In clear contrast, the microsecond kinetics of the $P680^+$ reduction exhibit sizeable KIE-values and were interpreted as arising from rearrangement of the hydrogen network in the environment of Y_Z, including specific proton transfer events [27,24].

The oxidized tyrosine, Yz^{OX}, is reduced by electron transfer (ET) from the Mn_4Ca complex within tens to hundreds of microseconds in the lower S-transitions and with a halftime of ~1.2 ms in the O_2-evolving step [35–37]. The Kok model [31] describes the light-driven cycling of the Mn_4Ca complex through its five oxidation states, S_0 to S_4, with focus on the accumulation of oxidizing equivalents by removal of electrons from the catalytic site. Later the mechanistic importance of proton transfer and release was pointed out repeatedly [38–41,16,3] and an extension of the classical S-state cycle was proposed, including electron and proton removal from the Mn complex [37,15,16,3]. The 'intrinsic proton-release pattern' describing the number of protons that are removed from the Mn complex in the four transitions $S_1\rightarrow S_2\rightarrow S_3\rightarrow S_0\rightarrow S_1$ has been shown to be 1:0:2:1 [42–44,41,45]. This is in accordance with the interpretation of the retarded $P680^+$ reduction kinetics in S_2 and S_3 as being a consequence of a positive net charge of the Mn complex [22]. While the $S_1\rightarrow S_2$ transition appears to be a pure electron transfer step, during $S_2\rightarrow S_3$ both one proton and one electron are removed from the Mn complex, leaving the states S_2 and S_3 singly positively charged (S_2^+ and S_3^+ [3]) relative to the dark-stable S_1 state. The $S_3\rightarrow S_0$ transition comprises removal of two protons and one electron, O_2 release and possibly also substrate water binding, leaving the S_0 state uncharged relative to S_1 (S_0^n and S_1^n [3]).

Photoacoustic (PA) techniques are capable of monitoring density changes associated with photoinduced reactions; the density changes may arise from heat release or volume changes [46–48]. Providing direct access to enthalpy changes, different photoacoustic approaches have been used to investigate a variety of photosynthetic systems of different origins [49,50]. Pioneering in this field was the work of Parson and coworkers using a capacitor microphone coupled directly to suspensions of non-oxygenic photosynthetic bacterial reaction centers. In an interval between 100 μs and 1 s volume changes could be measured, and contributions caused by heat release (enthalpy change) could be distinguished from contributions of non-thermal origin, e.g. volume changes of the protein [51,52]. Later gas-phase microphones were used to monitor dioxygen formation and thermal dissipation in photoacoustic experiments on intact leaves [53–56].

In a modified PA approach, called laser-induced optoacoustic spectroscopy (LIOAS), a pulsed laser was used for excitation and a transducer coupled mechanically to the sample cell containing the sample suspension detected the pressure wave. Time resolutions in the nanosecond and microsecond range became accessible by this method, whose application to suspensions of biological photoreceptors was established mostly by Braslavsky and coworkers [46,47].

With regard to PSII, LIOAS was applied to determine enthalpy changes, quantum yields and conformational volume changes associated with charge separation processes in the microsecond time domain [50]. Enthalpy and volume changes were found to vary for different PSII preparations. The volume change in the microsecond time scale was reported to be -16 Å^3 for PSII membrane particles from spinach [49], -9 Å^3 for manganese-depleted core particles of Synechocystis (at pH 6) [57] and -2 Å^3 for whole cells of Synechocystis [58]. As the ET from Y_Z to $P680^+$ is slowed down significantly in manganese-depleted PSII [59,60], the charge-separated state reached within 1 μs will differ from the state reached in intact PSII.

In the present study, we are aiming at a photoacoustic characterization of PSII membrane particles with an intact Mn complex in distinct oxidation states (S_i states) of the Mn complex. Volume changes with lifetimes of tens to hundreds of nanoseconds have been found for PSI of the cyanobacterium Synechocystis 6803 [61] and for D1–D2-Cyt b559 reaction center complex of PSII from higher plants [62]. For the first time, we resolve nanosecond volume changes for oxygen-evolving PSII, which display a pronounced dependence on the oxidation state of the Mn complex. These volume changes parallel the slow nanosecond kinetics. We discuss that specifically in the S_2 state, a distinct nuclear rearrangement precedes both the proton removal from the Mn complex and electron transfer to the oxidized tyrosine residue.

2. Materials and methods

2.1. Sample preparation

Measurements were carried out on highly active PSII membrane particles (≥1100 μmol O_2 per mg Chl and h, at 28 °C), prepared from spinach as described elsewhere [63,64] using Triton X-100 as an detergent as first described in Ref. [65]. Before use, the preparations were thawed for 2 hours on ice and resuspended in a buffer solution (pH 6.2; 1 M glycine betaine, 25 mM MES, 10 mM NaCl, 5 mM $CaCl_2$, and 5 mM $MgCl_2$). Standard PSII samples for photoacoustic measurements contained 180 μg Chl per mL and, if applicable, an exogenous electron acceptor DCBQ (2,6-dichlorobenzoquinone, 20 μM).

Prior to each series of PA experiments, the absorption of the PSII suspension at 532 nm was determined from an absorption spectrum recorded from 300 to 1000 nm (Cary 50 spectrophotometer, Varian). The scattering background was minimized by positioning the optical

cuvette directly in front of the detection diode with the measuring light passing the rough-surface sides of the cuvette. The remaining scattering background was removed by subtraction of a line, which had been chosen for zero absorption between 800 and 1000 nm. A solution of 0.07 g/L of BCP (bromocresol purple) at pH 6.2 exhibited a similar absorption at 532 nm (0.067 absorption units at 0.5 mm optical path length) as determined from the scattering-corrected spectra of the PSII membrane particles.

2.2. Photoacoustic measurements

A home-made layered prism cell [66] was used to minimize artifacts from light excitation of the microphone. The photoacoustic (PA) signal was detected by an ultrasonic transducer (2.25 MHz resonance frequency, V133-RM, Olympus NDT Inc., Waltham, MA), amplified (HVA-10M-60-F, FEMTO, Berlin), and recorded by a personal computer equipped with a 12-bit 7-MHz A/D card (PCI-1714U, Advantech, Taipei).

The PA experiment on PSII samples involved two types of ns-laser flashes:

(1) For induction of the photoacoustic signal, non-saturating measuring flashes from a Q-switched, frequency-doubled Nd:YAG laser were used (Continuum Minilite II; 532 nm, full width at half-maximum (FWHM) of 3–5 ns, flash-energy density of 50 μJ/cm^2 at the sample). The intensity of the non-saturating flashes was chosen such that the level of saturation was small, but partial saturation did occur.
In the absence of any saturation, the photochemical contribution to the PA signal normalized to the energy of the measuring flash would be maximal (maximal photochemical yield). The partial saturation, which we deduced from the intensity dependence of the PA signal, reduced the photochemical contributions to the PA signal by 13%, in comparison to a hypothetical signal amplitude without any saturation. (This means that about 13% of the photosystems are hit by two photons within the duration of the measuring flash but only the first photon can induce the photochemistry reflected in the PA signal.)
(2) For advancement in the S-state cycle, fully saturating flashes were provided by a second Nd:YAG laser (Continuum Inlite, 532 nm, FWHM of 5 ns, flash-energy density of ~4 mJ/cm^2).

These two types of flashes were applied always as pairs of (1) the non-saturating measuring flash and (2) the saturating flash, with a time delay of 6 μs between these two flashes. Within a time interval of 30 μs before and 30 μs after the measuring flash, the PA signal was recorded at a sample rate of 19.5 MS/s.

In the photoacoustic double-flash experiment, the dark-adapted PSII membrane particles were kept in a dark reservoir on ice and transferred to the thermostated cell by a peristaltic pump (Masterflex, Cole Parmer). Then a series of 20 double flashes each consisting of (1) the non-saturating measuring flash followed, with a time delay of 6.0 μs, by (2) the saturating laser flash. The time interval between two double flashes was 1.0 s. After each sequence of 20 double flashes, the PSII sample was exchanged. The sample reservoir contained sufficient PSII sample for collection of 25 flash series (each involving 20 double flashes) at each of the seven selected temperatures.

As a calorimetric reference, either a water-soluble dye (bromocresol purple, BCP; Na salt, Sigma) or PSII samples with a fully reduced pool of quinone molecules were employed as an intrinsic reference. The reduction of Q_A, Q_B, and Q_C [67] and of the other plastoquinone molecules present in the PSII preparation [68] ensures that the measuring flash cannot initiate reduction of the quinone electron acceptors so that the photon energy is mostly released by rapid thermal dissipation (<5 ns). The intrinsic reference was used instead of a reference dye in order to minimize inaccuracies that could result from the strong light scattering of PSII membrane particles. Reduction of the quinones was achieved by exposure to continuous background light from a light emitting diode (627 nm, 3 W of electrical power). To obtain the intrinsic reference signals at various temperatures, the PSII solution was filled into the thermostated sample cell (layered prism cell, formed by two glass prisms separated by a Teflon spacer to yield an optical path length of 0.5 mm; home-built cell holder thermostated electrically by means of Peltier elements, PKE 128 A 0020, Peltron GmbH, Germany). Then red background light was applied and 100 PA transients were recorded for excitation at a flash frequency of 2 Hz. After collection of 100 transients, the PSII sample was exchanged against a dark-adapted PSII sample.

2.3. Correction for miss events

A less-than-unity quantum yield for excitation of S-state transitions by saturating light flashes results in so-called misses (described by m, the miss probability). The probability for miss events typically is around 10%. Miss events prevent a fully synchronized advancement through the water oxidation cycle (S-state scrambling at higher flash numbers). A correction was approached (S-state deconvolution). For the determination of the miss parameter, m, two assumptions were made: *(i)* each PSII is in the dark-stable S_1-state before flash excitation and *(ii)* the fraction of PSII proceeding to the next S-state upon (double-)flash application is given by $(1-m)$. Extensive dark adaptation excluded the presence of a major fraction of PSII in the S_0-state; the used flash protocol excluded so-called double hits [31].

The absence of double hits (that is, advancement by two steps in the classical S-state cycle [31]) requires an explanation. A saturating light pulse provided by a xenon-flash lamp typically induces double hits, even for an FWHM of the flash-lamp pulse as short as 6 μs. Therefore the question arises of whether the non-saturating and the saturating flash spaced by 6 μs also could result in double hits. However we did not detect any indications for a significant double-hit probability in analysis of our double-flash experiments. We think that the double hits observed for a xenon-flash lamp largely result from the tail of the saturating flash-lamp pulse which is detectable for more than 100 μs after onset of the flash-lamp pulse. In our double-flash experiment however, the exciting photon flux is virtually zero already at 6.1 μs after the first laser flash so that the probability for double flashes is negligibly small.

Applying the model of Kok [31] and the mathematical approach described elsewhere [69], the four 'pure' PA signals—each attributable to PSII in one of the four (semi-) stable S states (S_1, S_2, S_3, and S_0)—were calculated from the PA signal traces measured at the 1st to 4th double-flash for a specific value of m (e.g. 10%) [69]. In a second step, the thereby obtained pure PA signals for the four different S states were used to simulate the PA signals of the 5th to 10th laser flash. The optimal value of m was determined by repeated variation of m and minimization of an error sum calculated for the 5 PA transients induced by the 5th to 10th double-flash.

2.4. Quantitative analysis of PA signals

The photoacoustic signal reflects a pressure wave induced by excitation of the PSII sample by the Laser flash. The pressure wave is formed due to (i) thermal dissipation of a distinct fraction, Q, of the energy of absorbed photons ($=h\nu$) and (ii) nuclear rearrangements that correspond to a non-thermal volume change, ΔV_e, of the PSII protein or its solvent shell. The total PA signal can be described as follows [48]:

$$H^S = \frac{C \cdot E_{\mathrm{abs}}}{\kappa_T}\left(\frac{\beta}{C_P \rho} Q + \frac{\Delta V_e}{h\nu}\right), \quad (1)$$

where E_{abs} is the total laser-pulse energy absorbed by the PSII sample. The constants κ_T, β, C_P, and ρ are the isothermal compressibility, the cubic thermal expansion coefficient, the specific heat capacity, and the solvent density, respectively. The instrumental constant, C, is determined

experimentally by comparison of a measured signal with that of a calorimetric reference [47,48]. The calorimetric reference is characterized by its ability to release 100% of the absorbed light energy within a time that is clearly shorter than the integration time of the experimental setup. For the reference signal, H^{Ref}, holds, $Q=1$ in Eq. (1) and $\Delta V_e=0$.

Kinetic information on transient species with lifetimes within the pressure integration time can be gained by a reconvolution-curve-fitting technique [70]. In this approach the time-dependent impulse response function (density and/or volume changes after photoexcitation) is described by a sum of single-exponential functions:

$$H(t) = \sum_i \frac{A_i}{\tau_i} \exp\left(-\frac{t}{\tau_i}\right), \tag{2}$$

with τ_i being the respective time constant of the ith reaction intermediate, and A_i its fractional amplitude. The measured signal is simulated by a time convolution of the impulse response, $H(t)$, with the instrumental response function. The latter corresponds to the reference signal, H^{Ref} (calorimetric reference dye or the intrinsic reference). The parameters A_i and τ_i can be varied to minimize the squared differences between the simulated and measured time courses (least squares curve-fitting).

Each fractional amplitude, A_i, consists of a contribution induced by heat release, Q_i, and a contribution due to structural volume changes, $\Delta V_{e,i}$ (see Eq. (1)). In aqueous samples these two contributions can be separated by means of temperature variation [47,48]. The factor $\beta/(C_p\,\rho)$, which determines the heat contribution to the photoacoustic signal (see Eq. (1)), depends strongly on temperature. In a temperature range between 0 °C and 30 °C, this temperature dependence can be simulated by a second order polynomial. Assuming the structural volume change, ΔV_e, and therefore the non-thermal part of the PA signal, V_R, is constant in this temperature range, the following relation can be used to estimate the values of Q_i and $V_{R,i}$ from the temperature dependence of A_i:

$$A_i(T) = \left(a + b\cdot T + c\cdot T^2\right) Q_i + V_{R,i}. \tag{3}$$

First the parameters a, b, and c were determined by simulating the temperature dependence of the calorimetric reference (either reference dye or intrinsic reference, $Q=1.0$; $V_R=0$). On these grounds, the values for the fraction of heat release, Q_i, and the structural volume change, $V_{R,i}$, were determined by simulating the temperature dependence of the amplitudes, A_i.

The absolute volume change per PSII, ΔV_e, may be estimated from the structural part of the PA signal, V_R, and the signal of the reference, H^{Ref}, via the following equation [71]:

$$\Delta V_e = \frac{h\nu\cdot\beta}{\rho\cdot C_P}\frac{\kappa_T^{(-8)}}{\kappa_T^{(20)}}\frac{V_R}{H^{Ref(20)}} = \chi\frac{V_R}{H^{Ref(20)}}. \tag{4}$$

In Eq. (4), the value of χ would equal 21.8 Å^3 if it were assumed that the properties of pure water at 20 °C are close to the properties of the herein used buffer ($\beta=206.6\ 10^{-6}$ 1/K, $C_p=4.1819$ J/g K, $\rho=998.23$ kg/m^3, and $\kappa_T^{(20)}=4.589\ 10^{-10}$ Pa^{-1} [72], $\kappa_T^{(-8)}=5.412\ 10^{-10}$ Pa^{-1}, where the superscripts '(−8)' and '(20)' relate to the values determined at −8 °C and 20°C, respectively). A control experiment revealed that this assumption is too approximative (see Refs. [73–75] and Fig. S1). For the herein used buffer containing glycine betaine at high concentration (1 M), a better estimate is provided by Eq. (5) (see also Fig. S1):

$$\Delta V_e = 31\pm 6\ A^3\frac{V_R}{H^{Ref(20)}}. \tag{5}$$

We emphasize that the *relative* magnitudes of the herein described volume changes are *not* affected by the uncertainties in the values of the thermoelastic parameters of the buffer medium.

3. Results

3.1. PA signals assignable to specific S states of PSII

By application of laser flashes (see Section 2.2) to initially dark-adapted PSII samples, the PSII was driven through its S-state cycle in a largely synchronized way and PA signals were recorded for each (preferentially populated) S-state. The first non-saturating laser flash induced the PA signal of PSII in which mostly the S_1 state was populated. The following saturating flash, applied only 6 µs after the non-saturating flash, excites essentially all PSII protein complexes and causes $P680^+Q_A^-$ formation in all the PSII that have not been hit before by the non-saturating flash; $P680^+Q_A^-$ formation is followed by Y_Z oxidation and then by the $S_1\rightarrow S_2$ transition. By means of this unconventional double-flash protocol, on the one hand, the PA signal can be measured for a non-saturating flash and, on the other hand, the number of PSII that after application of one double-flash proceeded by two steps in the classical S-state cycle was kept at a negligibly small level (negligible double-hit probability). When the next non-saturating flash was applied, most of the photosystems had reached the S_2 state and the corresponding PA signal was recorded. By the third double-flash pair, the PA signal of PSII predominantly in the S_3 state was recorded and a major PSII fraction was propelled to the S_0-state, and so on.

The pressure wave induced by each laser flash needed about 1.5 µs to travel to the transducer. In Fig. 2, the PA signals induced by the non-saturating measuring flashes in PSII that had been exposed to zero, one, two, or three saturating laser flashes are shown. Thus a prominent oscillation starting 1.58 µs after the laser-flash marks the beginning of the PA signal detected by the transducer. As clearly visible in Fig. 2, the signals recorded for the second and third non-saturating flash (flash-2 and flash-3) differ significantly from the flash-1 signal. In Fig. 3, the flash-number dependencies of the transducer signal at 1.95 µs (~50 ns after the first PA maximum at 1.90 µs) and 5.95 µs (as a measure of the plateau level at later times) are shown. These amplitude exhibit a clear period-of-four oscillation indicating the flash-number dependence of the PA signal is assignable to reactions at the PSII donor side.

3.2. Scattering artifact

A smaller, strongly damped oscillation is visible in the transducer signal immediately after excitation by the laser-flash (Fig. 2, maximum at ~200 ns). This laser-flash artifact is caused by scattered light hitting the transducer membrane directly. The thereby induced oscillation of the transducer was strongly damped and therefore neglected in our numerical analysis. (We note that the ratio between the dominating signal contributions from PSII and the flash artifact became more

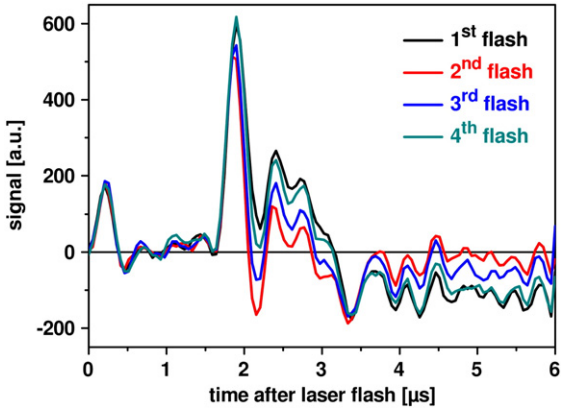

Fig. 2. Time courses of photoacoustic signals as induced by the first to fourth laser flash. The shown PA transients were obtained by averaging the individual transients of 300 flash trains; each flash train was applied to fully dark-adapted PSII membrane particles.

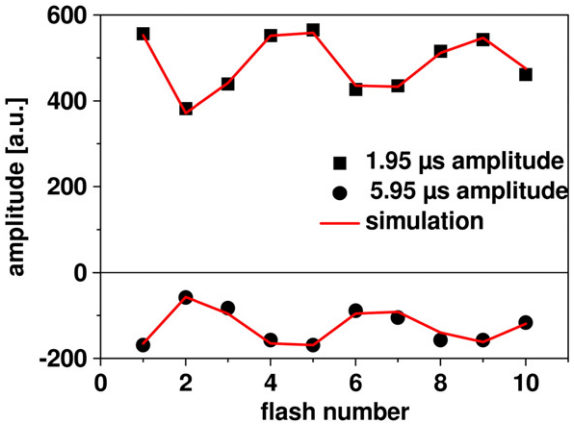

Fig. 3. Flash pattern of the photoacoustic signal at 1.95 µs (squares) and at 5.95 µs (dots). A sequence of 20 double flashes was applied to dark-adapted PSII membrane particles (at 25 °C); the amplitudes of PA signal at 1.95 µs and 5.95 µs after application of the non-saturating ns-laser flash are shown. The period-of-four pattern results from cycling of the Mn complex through its reaction cycle (S-state cycle) and indicates an S-state specific contribution to the PA signal. The dampening of the oscillation pattern results from miss events. The red lines represent simulations with a miss parameter of 10.0%.

unfavorable at low temperatures but still did not affect the outcome of our analysis significantly.) In addition, a pressure disturbance is caused by the scattered light which is reflected at the border of prism and sample compartment. The reflection of this pressure wave is superimposed to the main PA signal resulting in a first minimum at ~3.4 µs. This contribution from reflections of the pressure wave explains minor systematic deviation between signal and simulation (discussed further below), beginning about 3.3 µs after application of the laser flash.

3.3. Correction for imperfect S-state transitions (deconvolution)

By application of saturating laser flashes, the PSII was stepped largely synchronously through its reaction cycle. However, desynchronization due to so-called miss-events cannot be avoided completely. The miss parameter, *m*, describes the probability that laser-flash application does not result in advancement in the S-state cycle. Numerical corrections based on the Kok model [31,69] were employed to compensate for S-state desynchronization resulting in the PA transients for PSII in 'pure' states of the PSII donor side, which are shown in Fig. 4. For details of the correction procedure, see Section 2.3.

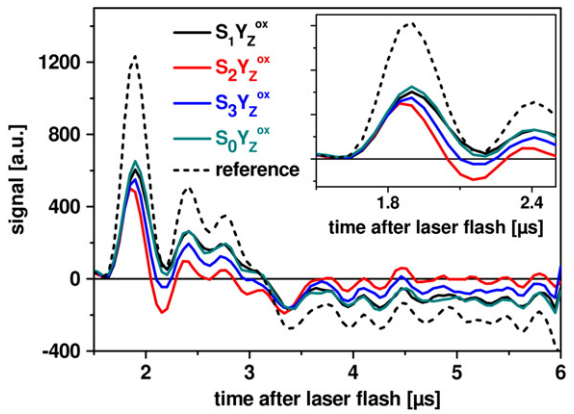

Fig. 4. Photoacoustic signals of PSII in the states S_1, S_2, S_3, and S_0 (S-state before application of the ns-Laser flash). The shown transients were corrected for miss events (miss parameter of 10.0%). The signal of an intrinsic reference is shown as a dotted line. The inset shows the first oscillation of the PA signal on an expanded timescale.

The magnitude of *m* was determined by simulation of the pattern of PA amplitudes measured for the first ten double flashes as described in Section 2.3. As expected [76,77], the determined miss parameter exhibited a slight temperature dependence. The maximal *m*-value of 12.8% was reached at 0 °C. Between 10 °C and 30 °C the miss parameter was close to 10%.

3.4. Temperature dependence

The PA signals corrected for miss events are shown in Fig. 4. Visual comparison to the signal of the clearly larger signal of the intrinsic reference (dashed line in Fig. 4) suggests that, in all S states, a major fraction of the absorbed light energy is not released in form of heat but chemically stored by formation of the $Y_Z^+Q_A^-$ radical pair. For a more detailed analysis, PA signals were collected at temperatures ranging from 0 °C to 30 °C and corrected for miss events. The resulting transients are shown in Fig. 5.

Eq. (3) predicts that signal contributions arising from heat release decrease continuously with decreasing temperature, whereas signal contributions reflecting density or volume changes (of PSII) are temperature independent and thus may dominate at low temperatures. The superposition of thermal and volume contributions to the PA signal of PSII can explain the pronounced changes in the shape of the PA signals with decreasing temperatures (see Fig. 5). In the following section, we will approach a fully quantitative analysis.

3.5. Monophasic and biphasic volume change

We describe the response of PSII to the exciting laser pulse by a response function, *H(t)*, and simulate the PA signal be convolution of *H(t)* and the signal obtained for the (intrinsic) calorimetric reference, as outlined in Section 2.4. After excitation of PSII by the laser flash, the excited antenna state decays radiatively (fluorescence), non-radiatively by thermal deactivation), and by initiation of the ET steps, which result in formation of the $P680^+Q_A^-$ radical pair. All these processes are clearly faster (<<10 ns) than the time response of the PA experiment. For numerical reasons, we model the kinetically unresolved prompt response of PSII by an exponential component with a time constant of 10 ns (τ_1 in Eq. (2)). We note that for excitation with a picosecond laser flash, the formation of the initial $P680^+Q_A^-$ radical pairs is essentially completed within about 1 ns [78]. By using a τ_1-value of 10 ns, we take into account that we excite with a ns-laser flash and, more importantly, avoid computational problems. In any event, the precise τ_1-value is fully uncritical for the modeling of the PA time courses (for τ_1 smaller than about 30 ns).

This modeling approach provides a fully adequate description of the PA signal for PSII in the S_0 and S_1 state (Fig. 6A), suggesting that the P680-Y_Z electron transfer cannot be resolved in the PA signal. We note that after appropriate normalization, the simulated PSII signal (which models the experimental PSII signal very well) and the reference signal are found to be largely identical, as predicted for a fast PSII response.

However for PSII in the S_2 state and in the S_3 state, the description by a mono-exponential (prompt) response of PSII results in major differences between simulated and experimental PA signal, as clearly visible in Fig. 6B. The PA signal at the minimum of the first oscillation (at 2.2 µs) was negative in the S_2 and S_3 state (at all temperatures), whereas it exhibited positive values for the reference signal (dashed line). This implies that simulation of the PA signals of PSII in the S_2 and S_3 state requires a response function, *H(t)*, comprising two components of opposite signs. Thus we approached a bi-exponential description of the PSII response to the laser flash involving a prompt response ($\tau_1 = 10$ ns) and a delayed response with a time constant, τ_2, of several hundred nanoseconds. The precise value of τ_2 and the amplitudes of the two exponential contributions (A_1 and A_2 in Eq. (2)) were obtained by curve-fitting. The assumption of a prompt and delayed PSII response facilitated high-quality simulations of the PA signal

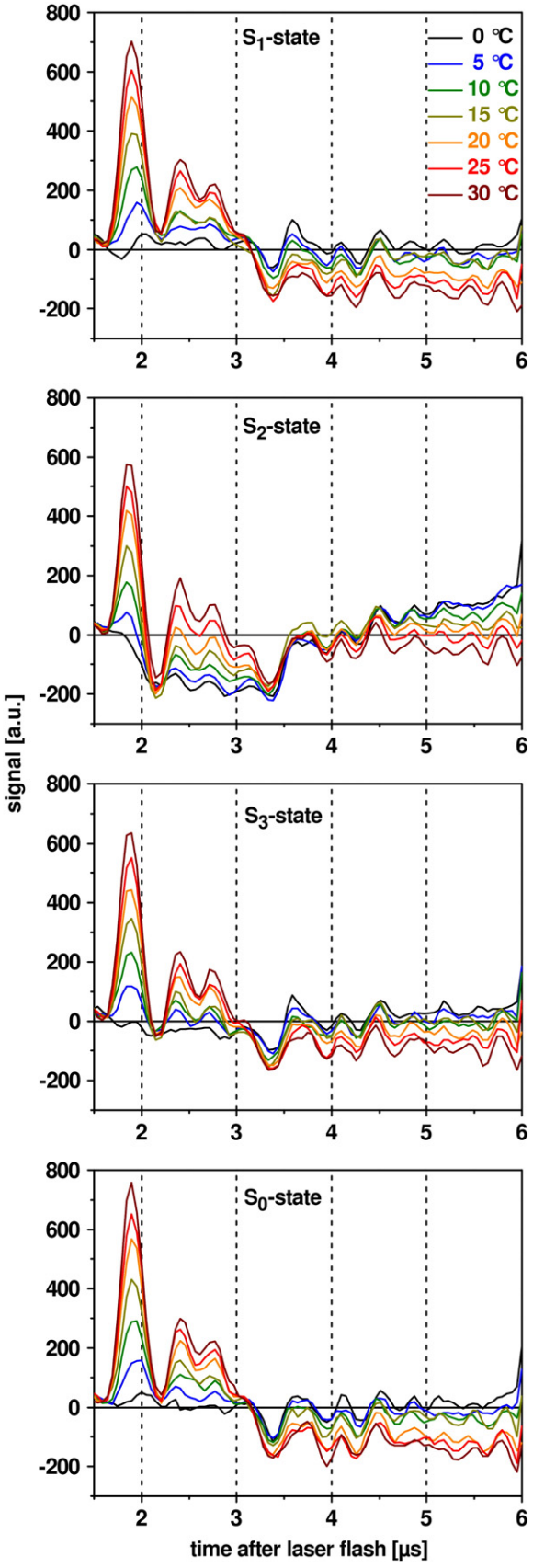

Fig. 5. Temperature dependence of photoacoustic signals of PSII membrane particles in the S_1, S_2, S_3, and S_0 state. The shown transients were corrected for miss events. The value of the miss parameter was close to 10% but was found to depend slightly on the temperature (0 °C, 12.8%; 5 °C, 11.6%; 10 °C, 9.5%; 15 °C, 10.6%; 20 °C, 9.4%; 25 °C, 10.0%; 30 °C, 10.2%). At each temperature, three hundred flash trains were applied.

measured for PSII in the S_2 or S_3 state, as illustrated in Fig. 6B. Values obtained by curve-fitting for A_{prompt} (A_1 in Eq. (2)), $A_{delayed}$ (A_2), and $\tau_{delayed}$ (τ_2) are presented in Figs. 7 and 8.

3.6. Thermal and structural contributions to the PA signal

The temperature dependence of the amplitude, A_{prompt}, is shown in Fig. 7A. Simulation based on Eq. (3) revealed the fraction, Q, of absorbed energy that is released promptly as heat (in percent of the heat being released promptly by the intrinsic reference; open symbols in Fig. 7). Values for Q_{prompt} determined for the different S states varied between (70 ± 11)% and (77 ± 12)% and were within the error indistinguishable (see Table 1). The structural (non-thermal) contribution to the prompt part of the signals, $V_R^{(prompt)}$, had a negative value for all four S states and thus corresponds to a slight contraction. Per PSII, values between -6 ± 3 and -10 ± 4 Å^3 were calculated using Eq. (5).

The delayed PSII response is of special interest. Fig. 7B shows the fractional amplitudes, $A_{delayed}$, of the delayed PSII response in the S_2 and S_3 state, which is characterized by time constants of hundreds of nanoseconds (Fig. 8). The negative value of $A_{delayed}$ (negative at all temperatures) implies a density increase of PSII (negative value of ΔV_e), which corresponds to a sizeable contraction. The values obtained for Q and ΔV_e are summarized in Table 1.

The activation energies of the reactions (or processes) observable after laser-flash excitation of PSII in the S_2 or S_3 state were determined from the respective Arrhenius plot in Fig. 8 and are summarized in Table 1.

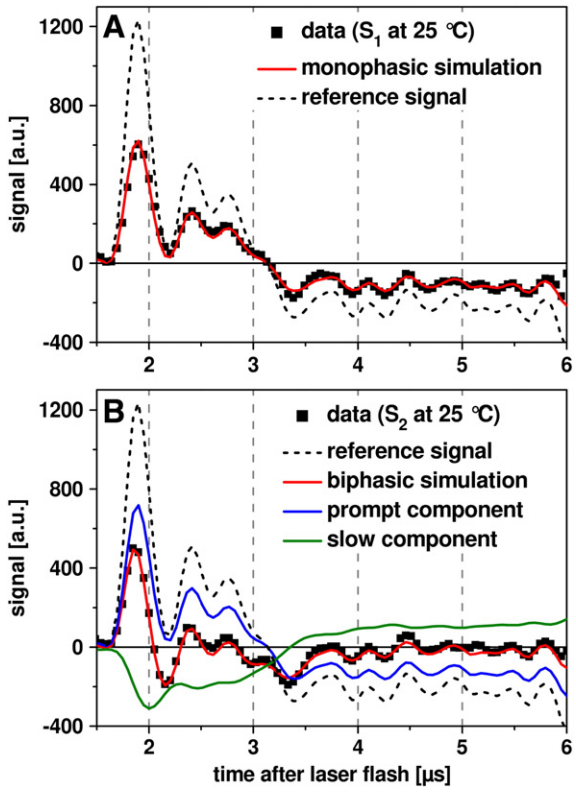

Fig. 6. Simulation of the photoacoustic signal of PSII in the S_1 state (A) and in the S_2-state (B). Symbols, experimental data. Red line, simulation using a monophasic model in (A) and a biphasic model in (B). The shown data was collected at 25 °C; the curve-fitting involved an iterative re-convolution (see Section 2.4). In the biphasic model, the total PA signal consists of two contributions: a prompt component (blue line) and a slow component characterized by a time constant of about 350 ns (green line). The dashed line shows the reference signal, which was used as system response in the simulation of the PA transients. In A, the monophasic model (prompt component only) provided a fully adequate description.

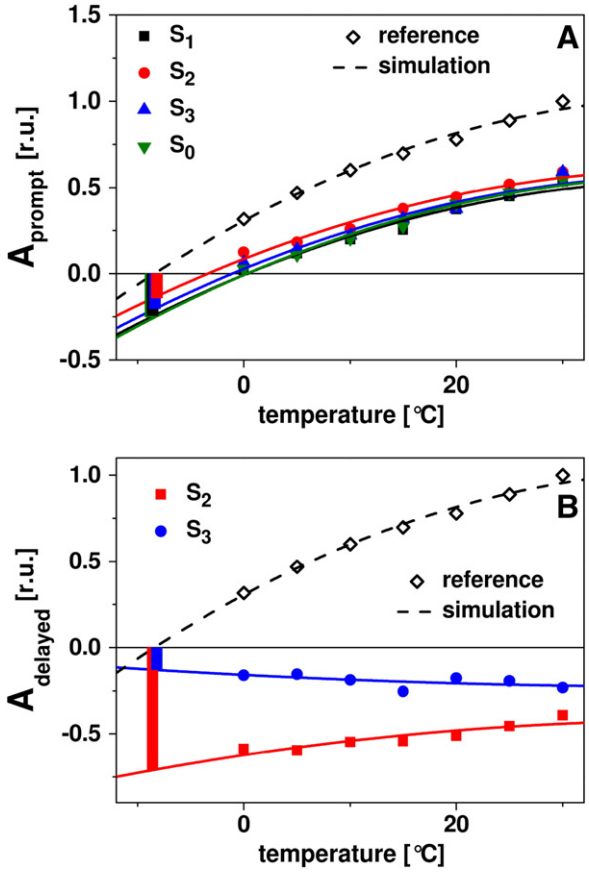

Fig. 7. Temperature dependence of the amplitudes of the fast (prompt) component of the PA signal (in A) and of the slow component (in B). The amplitudes were obtained by simulations that involved an iterative re-convolution (see Section 2.4; data ranging from 1.59 μs to 6.0 μs was used in the curve-fitting). Only for the PA signals of PSII in the S_2 and S_3 state, a biphasic simulation was required, which in addition to the prompt component (present in all S states) involved a slow component (200–900 ns). The amplitudes of the slow component are shown in panel B; the corresponding time constants are shown in Fig. 8. The open symbols in A and B indicate the amplitudes determined for the (prompt) response of the intrinsic reference. The lines were obtained by curve-fitting (Eq. (3), see Section 2.4). The lengths of the filled bars correspond to the magnitudes of the structural volume changes (V_e in Table 1) which can be calculated from the extrapolated PA amplitudes at −8 °C (see Eqs. (3) and (4) in Section 2.4).

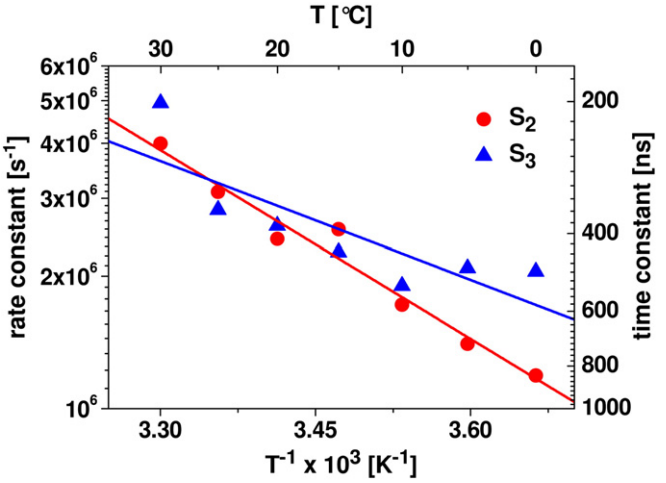

Fig. 8. Arrhenius plots of the rate constants of the slow component in the PA signals detected for PSII particles in the S_2 and in the S_3 state. The rate constants (filled symbols, left scale) or time constants (filled symbols, right scale) were determined by simulation of the PA transients shown in Fig. 5. The straight lines were obtained by simulations yielding activation energies of 285 ± 50 meV (in S_2) and 180 ± 110 meV (in S_3). The error ranges correspond to the estimated 2σ confidence interval. (We note that the value of the latter activation energy likely is meaningless. The uncertainty in the time constant values is so high that the prevalence of an Arrhenius-like temperature dependence cannot be concluded from the data.).

4. Discussion

4.1. Photoacoustic detection of initial and delayed contraction

4.1.1. Energy storage and quantum yield

Photoacoustic experiments can provide the fraction of the photon energy that is stored in form of chemical energy by the photosystem. This aspect is not in the focus of the present investigation, but discussed for completeness. The fraction of the energy of one 532 nm photon that is released as heat promptly was about 74% (averaged over the four S states). This would mean that only 26% of 2330 meV, that is, 600 meV would be stored in the $[P_{680}\leftrightarrow Y_Z]^+Q_A^-$ state, if the quantum yield were unity. Comparison of the value for E_{stored} of 600 meV to the one of 1100 meV determined by Delosme for excitation with red light [79] suggests that in our investigation the effective quantum yield for excitation at 532 nm was about half as large as reported by Delosme [79]. A quantum yield close to 100% has been reported for charge separation in PSII core complexes excited with red light [57]; a quantum yield of 55% thus would result from our study. Grabolle indeed found that the quantum yield may be as low as 50% for excitation of PSII membrane particles at 532 nm [80] possibly explainable by inefficient energy transfer after excitation of carotenoids at 532 nm. A relatively low quantum efficiency for excitation with green light was found already in 1946 by Emerson and coworkers [81,82]. Also the neglect of fluorescence emission in our analysis could contribute to the low value for photochemical energy storage.

4.1.2. Initial contraction in all S states

The PA signals measured on dark-adapted PSII membrane particles with intact manganese complex exhibit a clear S-state dependence. While prompt volume contractions of about −8 Å^3 (Table 1) are observed for all four S states, prominent density changes with lifetimes in the hundreds of nanoseconds are observed only for excitation of PSII in the S_2 and S_3 state.

Assuming that in our investigation the quantum yield had been 55%, we calculate a ΔV_e value of about −15 Å^3, which is in reasonable agreement with previously determined values of −16 Å^3 for $[Y_Z^+Q_A^-]$-formation for PSII membrane particles from spinach [49] and −9 A^3 for $[P680^+Q_A^-]$-formation in manganese-depleted PSII core particles [57]. This contraction has been proposed to result from electrostriction induced by formation of uncompensated charges at the Q_A-site (Q_A^-)

Table 1
Heat release in percent of the photon energy (Q) and volume changes, ΔV_e, as derived from the temperature dependence of the PA signals detected for PSII in S_1, S_2, S_3, and S_0. Processes faster than 50 ns (prompt, fast component) and processes in the range of hundreds of nanoseconds (delayed, slow component) were detected. The values given for the activation energy, E_A, were determined from the Arrhenius plots in of Fig. 8. The indicated time constant corresponds to a temperature of 25 °C. The given values are not corrected for the quantum yield for excitation at 532 nm, which may be as low as 55%. The error ranges correspond to the 2σ confidence interval of the respective fit parameter. For the ΔV values (volume changes), the given error range includes also a (dominating) contribution from the uncertainty in the value of $(\beta\rho)/C_p$, see Eq. (5) and Fig. S1.

	$S_1Y_Z^{ox}$	$S_2Y_Z^{ox}$	$S_3Y_Z^{ox}$	$S_0Y_Z^{ox}$
Q_{prompt} [%]	73.8 ± 11.4	70.2 ± 10.2	73.2 ± 14.4	77.3 ± 10.8
$Q_{delayed}$ [%]	–	27.0 ± 11.8	−9.1 ± 10.6	–
ΔV_{prompt} [A^3]	−9.2 ± 3.6	−5.5 ± 2.9	−8.0 ± 4.4	−9.8 ± 3.4
$\tau_{delayed}$, 25 °C [ns]	–	320	350	–
$\Delta V_{delayed}$ [A^3]	–	−26.6 ± 5.1	−4.8 ± 3.2	–
E_A [meV]	–	285 ± 50	180 ± 110	–

and at the donor side of PSII ($P680^+$ or Y_Z^+) [57,83], as discussed further below in more detail.

4.1.3. Delayed contraction in S_2 and S_3 (~350 ns)

The amplitude of the delayed phase, $A_{delayed}$, of the PA signal is found to be negative at *all* investigated temperatures in the S_2 and in the S_3 states (Fig. 7B), providing evidence for a contraction of PSII (density increase) in the time range of hundreds of nanoseconds ($\tau_{delayed} = 200–900$ ns). The contractions are observed specifically for laser-flash application in the S_2 and S_3 state. The volume change is clearly more pronounced in the S_2 state than in the S_3 state. This finding of an S-state specific volume change represents a central result of our investigation.

Evaluation of the heat release associated with the nanosecond contraction in the S_3 state yields a negative value of −9% (Table 1) but is equal to zero within the 2σ uncertainty range. Interpretation of the temperature dependence of $A_{delayed}$ for Laser-flash application in the S_2 state, however, is not straightforward. The value of +27% (in Table 1) is unreasonably high. It is conceivable that the underlying process is not adequately described by a single-exponential function. Poor estimation of time-constant values resulting from choice of a too simple model could influence the temperature dependence of $A_{delayed}$ strongly. Alternatively, the strong temperature dependence could be an indication that the magnitude of the structural volume change is temperature dependent. For the photoactive yellow protein (PYP), the contraction associated with formation of the pR intermediate has been found to be two times larger at 0 °C than at 20 °C [84].

In conclusion, definitive conclusions on the enthalpy changes associated with the volume changes that occur with time constants of about 350 ns (at room temperature) cannot be drawn. However, this uncertainty does not affect our central conclusion. After $S_2Y_Z^{ox}$ and $S_3Y_Z^{ox}$ formation a contraction of PSII protein is observed which is especially pronounced for $S_2Y_Z^{ox}$.

4.2. Origin of observed contractions

4.2.1. Assignment to PSII processes detected previously

It is well established that the reduction of the primary electron donor of PSII, P680, by Y_Z is multiphasic and proceeds mainly in the nanosecond time domain [22,23,85,34,26–30,24]. For PSII in S_0 and S_1, absorption changes in the near infrared (~820 nm) monitoring $P680^+$ reduction are dominated by a fast decay component with lifetimes of 20–60 ns [22,23]. The prompt contraction in the S_0 and S_1 state thus arises from a $[P680/Y_Z]^+Q_A^-$ state in which $P680^+$ is almost completely re-reduced by Y_Z. (We note that the temporal kinetics of these fast processes cannot be resolved in our PA experiment. Whereas the rate constants remained unresolved, the magnitude of the associated volume changes could be estimated.) For the $P680^+$ reduction preceding the $S_2 \rightarrow S_3$ and $S_3 \rightarrow S_0$ transitions however, near-IR absorption data revealed a multiphasic $P680^+$ reduction with two distinguishable kinetic components in the sub-microsecond domain. For the faster one, a time constant of about 50 ns was reported whereas a value close to 300 ns was determined for the slower one. To explain this multiphasic behavior it was proposed that a sequence of relaxation processes shifts the redox equilibrium between $P680^+Y_Z$ and $P680Y_Z^{ox}$ toward the latter state [24] (see Fig. 9). Not only the time-constant values at room temperature but also the activation energies reported for the "slow" nanosecond kinetics of $P680^+$ reduction (280 ± 50 meV in S_2; 240 ± 80 meV in Ref. [30], but see also Ref. [23]) are very similar to the corresponding values we determined herein in the PA experiment for the delayed contractions (following the initial $S_2Y_Z^{ox}$ and $S_3Y_Z^{ox}$ formation (Table 1). Our results thus imply that the previously observed relaxation, i.e. the lowering of the ΔG level of the Y_Z^{ox} state relative to $P680^+$, is associated with a nuclear rearrangement that amounts to a contraction of the PSII protein.

4.2.2. Fast contraction by electrostriction

Before discussing the slow relaxation (~350 ns) in more detail, we will consider the physico-chemical origin of the fast component. The PA analysis suggests that the initial formation of the $[P680/Y_Z]^+Q_A^-$ radical pair is associated with an apparent contraction (density increase) of the PSII protein complex or (clearly less likely) of its solvent shell by about 15 Å^3. The magnitude amounts to roughly one half of the mean volume of a water molecule (~30 Å^3 in liquid water) and thus is exceedingly small in comparison to the total volume of the PSII complex. The magnitude of the contraction appears to be similar in Mn-depleted PSII [57] and in PSII with an intact Mn complex (herein and ref. [49]).

In all photosystems investigated so far [48,50] and also in synthetic molecular systems [86,87], a contraction has been found to be associated with formation of largely uncompensated charges by electron transfer. For molecules in an aqueous electrolyte, rearrangement of the surrounding ion shell in response to 'charging' of the molecule may render the electrolyte more compact (density increase) [88–90,86,48]. Yet in PSII, the charged cofactors (Q_A^- and at the donor side, $P680^+$ or Y_Z^+) are not close to the protein–solvent interface so that a density increase by rearrangement of ions in the solvent shell is unlikely to contribute significantly. However by subtle movements of charged or polar protein groups, including the numerous water molecules detected in PSII, an analogous compaction may occur in the protein interior. This compaction has been described as electrostriction using a continuum model of a protein with homogeneous elasticity properties [52,83]. Even though the continuum model represents a coarse approximation, qualitatively the electrostriction picture could be appropriate for explaining the volume change associated with formation of the $[P680/Y_Z]^+Q_A^-$ radical pair.

4.2.3. Slow contraction by S-state specific structural changes

While a small initial contraction of comparable magnitude is observed for PSII in the S_0, S_1, S_2, and S_3 state, the slow contraction (200–900 ns) is clearly S-state dependent. The slow contraction was not detectable in the states S_0 and S_1. In the S_3 state, its magnitude was clearly smaller than in the S_2 state. Relative to charge in the dark-stable S_1 state, the Mn complex is positively charged in *both* the S_2 and in the S_3 state (see Refs. [42,91,41,16,3] for a literature review) suggesting that it is *not* the charge state of the Mn complex that causes the especially pronounced contraction for PSII excited in the S_2 state. The magnitude of the slow contraction in the S_2 state, which likely exceeds 40 Å^3 (after correction for a low quantum yield), is clearly larger than the contraction assigned to the electrostriction-type response likely associated with formation of Q_A^- *and* $[P680/Y_Z]^+$. Most likely the events underlying the slow contractions are unrelated to the electrostriction-type response discussed further above for the fast contraction upon $[P680/Y_Z]^+Q_A^-$ formation. Based on the clear S-state specificity, we propose that the slow contraction (200 − 900 ns) observed specifically in the S_2 state ($-\Delta V$ of about 50 Å) and S_3 state ($-\Delta V$ of about 9 Å) roots in nuclear rearrangements relating directly to the Mn complex and the water network connecting the Mn complex with Y_Z, as it is schematically shown in Fig. 1.

4.2.4. Hypothesis: dual role of the Y_Z^+ relaxation ladder in the S_2 and S_3 state

In 2004, Renger [24] summarized results obtained by investigations on the multiphasic $P680^+$ reduction kinetics (for references, see Introduction section). Fig. 9 serves as an illustration of both Renger's interpretation and of our complementary viewpoint, as outlined in the following.

(1) $<Y_Z>_{initial}$. The fast component in the $P680^+$ reduction kinetics (~30 ns) is assigned to non-adiabatic Markus ET from Y_Z to $P680^+$ [24], which possibly is coupled to a shift of the Y_Z-proton to nearby His190 (see Introduction section, Fig. 1). The multiphasic $P680^+$

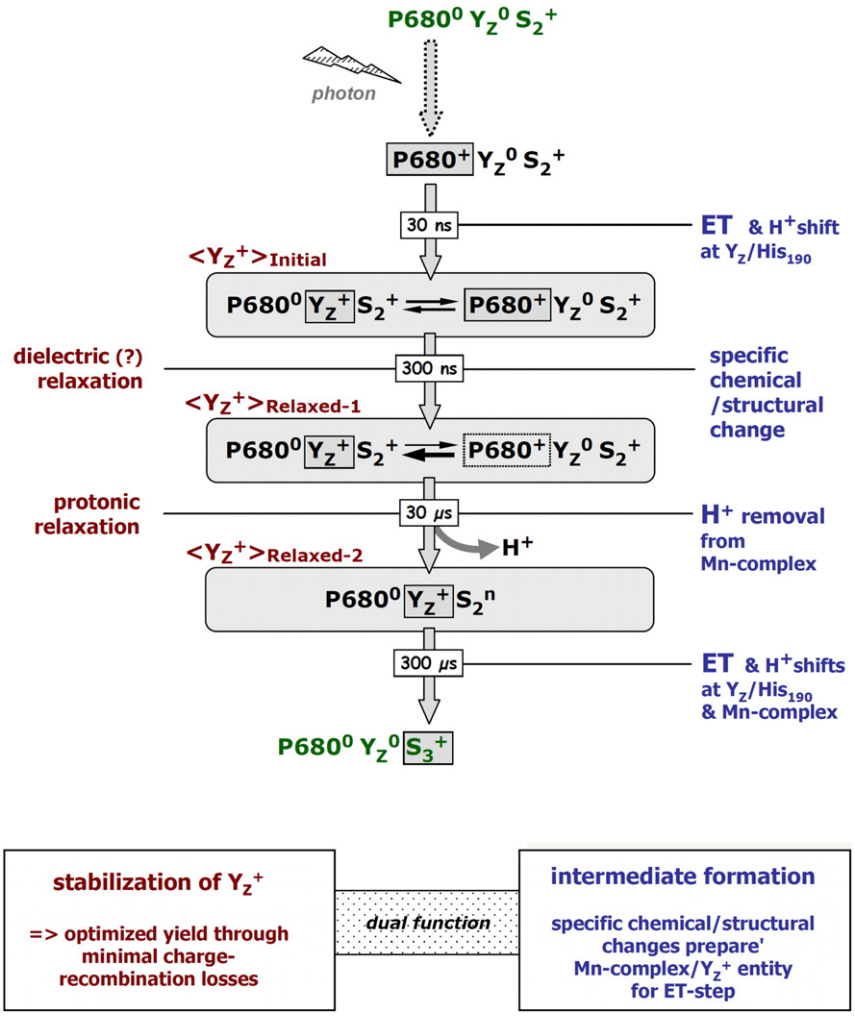

Fig. 9. Proposed sequence of events at the donor side of PSII after flash excitation in the S_2 state. Several steps may be viewed either as mere relaxation steps (assignments on the left side) or as formation of specific intermediate states (assignments on the right side). It is proposed that these two points of view are complementary, each addressing one side of the dual functional role of the respective processes. The expression 'dielectric relaxation' is marked by a question mark because it could be misleading to denote specific structural changes as a dielectric response.

reduction kinetics indicate that the ΔG^0 of this fast 30-ns-ET is low so that in the $<Y_Z^+>_{initial}$-state (see Fig. 9) of the PSII ensemble, $P680^+$ is present in a major PSII fraction (Fig. 9).

(2) $<Y_Z>_{relaxed\text{-}1}$. The slow nanosecond component in the $P680^+$ reduction kinetics (~300 ns) implies a pronounced shift of the redox equilibrium from the $P680^+Y_Z^0$ state toward the $P680^0Y_Z^+$ state, which can be viewed as a stabilization of the oxidized Y_Z by energetic relaxation, that is, stabilization by lowering of the corresponding free-energy level. Thereby the $<Y_Z^+>_{relaxed\text{-}1}$-state of the PSII ensemble is reached. In ref. [24], this process was denoted as 'dielectric relaxation' and assumed to originate from 'protein dynamics and cascades of relaxation processes'. We advocate an alternative explanation. The PA results imply that the observed energetic relaxation is associated with nuclear rearrangement which results in a contraction by about 50 Å^3. As a clearly smaller contraction is observed in the S_3-state (and none in S_0 and S_1), we assume that after Y_Z^{ox} formation, a specific chemical/structural change takes place which involves the Mn complex and its vicinity (Fig. 1). This chemical/structural step proceeds (necessarily) energetically downhill so that the free-energy of the radical-pair state is lowered and Y_Z^{ox} is further stabilized. Therefore this step can be viewed as an energetic relaxation. In conclusion, the process in the slow nanosecond domain is assigned to both, energetic relaxation and a specific chemical/structural change. The energetic relaxation corresponds to a stabilization of Y_Z^{ox} and thus reduces the likelihood for recombination of the cation radical at the donor side with the Q_A^- anion at the acceptor side of PSII [92–94,77,95]. By chemical/structural changes an intermediate state of the Mn complex and its environment is formed which represents the first step toward the subsequent proton removal from the Mn complex and electron transfer to Y_Z^{ox}.

(3) $<Y_Z>_{relaxed\text{-}2}$. The next step in the relaxation ladder of Fig. 9 is the formation of the $<Y_Z^+>_{relaxed\text{-}2}$-state, as concluded from the microsecond components of the $P680^+$ reduction kinetics. The herein presented PA results do not relate to processes in this time domain. We hypothesize that the 'protonic relaxation' assigned to $<Y_Z^+>_{relaxed\text{-}2}$-formation [26–29,24] is explainable by deprotonation and removal of a specific proton from the Mn complex, as detailed elsewhere [15,16,3,96]. Again a dual role of this step is encountered: (i) energetic relaxation reduces the likelihood for charge recombination losses further and (ii) a chemical step (deprotonation and proton relocation) facilitates the subsequent electron transfer from the Mn complex to Y_Z^{ox}.

The first step in the $S_3 \rightarrow S_4$ transition of PSII can be described in an analogous way. However, the chemical/structural change involved in

formation of $\langle Y_Z^+ \rangle_{\text{relaxed-1}}$ will be a different one because the PA results suggest a clearly smaller volume change.

The present PA investigation provides evidence that the 'dielectric relaxation' described previously [24] corresponds to structural change that, all in all, amounts to a contraction of the PSII protein. More specific atomistic information on the suggested structural change is still lacking. To provide the flavor of conceivable chemical/structural changes in the $Y_Z^{ox}S_2$-state, we will discuss briefly two specific but presently largely hypothetical scenarios.

(i) Based on X-ray absorption results [97,98,3] (but see also [99]), we proposed that in the $S_2 \rightarrow S_3$ transition, a water molecule or a hydroxide ($O^{(i)}H$), which is coordinated to a specific Mn ion ($Mn^{(i)}$), deprotonates and is transformed into an oxide bridging between $Mn^{(i)}$ and $Mn^{(ii)}$; concomitantly an open coordination site at $Mn^{(ii)}$ is filled by $O^{(i)}$ so that the coordination geometry of $Mn^{(ii)}$ is changing from being five-coordinated to six-coordinated (see Eq. (6)).

$$Mn^{(i)}\text{–}O^{(i)}H\text{.....}\text{–}Mn^{(ii)} + B^- \rightarrow Mn^{(i)}\text{–}O^{(i)}\text{–}Mn^{(ii)} + B\text{–}H \qquad (6)$$

The five-coordinated $Mn^{(ii)}$ was proposed to correspond to Mn^1 in Fig. 1 [11], as also suggested by computational studies [12,100,101]. Filling of the open coordination site at $Mn^{(ii)}$ and formation of a additional μ-oxo bridging between Mn ions will render the $Mn_4Ca(\mu\text{-}O)_5$ core of the Mn complex clearly more compact. To explain the PA results, we now assume that oxidation of Y_Z induces deprotonation of the $Mn^{(i)}$–$O^{(i)}H$ and transfer of the proton to a nearby base (B^- in Eq. (6)), e.g. the Asp61 in Fig. 1. Due to the relatively high structural flexibility of proteins (high elasticity), the compaction of the $Mn_4Ca(\mu\text{-}O)_5$ core (Eq. (6)) and changes in the H-bonding network shown in Fig. 1 could translate into a contraction of the PSII protein that is detectable in the PA experiment.

(ii) Siegbahn proposed for the $S_2 \rightarrow S_3$ transition an alternative structural change [12,18]: a water molecule from outside of the first Mn-coordination sphere deprotonates and fills the open coordination site at Mn^1 by getting into a bridging position between Mn^1 and the Ca ion. The volume of a solvated water molecule is close to 30 $Å^3$. The 'void' created by moving of an outer-sphere water into the open coordination site could result in a corresponding contraction of the PSII. To explain the PA results, we now assume that deprotonation of the outer-sphere water and the described nuclear rearrangements happen within about 300 ns after Y_Z^{ox} formation in the S_2 state.

The two scenarios described above merely serve as an illustration that distinct chemical/structural changes *could* explain the observed contraction upon Y_Z^{ox} formation in the S_2 state. Future computational and experimental investigations may provide more detailed insights which eventually may facilitate identification (at the atomic level) of the nuclear rearrangements whose existence is implied by the herein reported PA results.

Acknowledgements

Financial support by the European Union (EU, 7th framework program, SOLAR-H2 consortium) and the Bundesministerium für Bildung und Forschung (BMBF, "H_2 design cell" consortium) is gratefully acknowledged. We thank Dr. M. Haumann for stimulating discussion and M. Fünning for skilled preparation of PSII membrane particle.

Appendix A. Supplementary data

Supplementary data to this article can be found online at http://dx.doi.org/10.1016/j.bbabio.2012.04.017.

References

[1] R.E. Blankenship, Molecular Mechanisms of Photosynthesis, Blackwell Science, Oxford, England, 2002.
[2] J.P. McEvoy, G.W. Brudvig, Water-splitting chemistry of photosystem II, Chem. Rev. 106 (2006) 4455–4483.
[3] H. Dau, M. Haumann, The manganese complex of photosystem II in its reaction cycle—basic framework and possible realization at the atomic level, Coord. Chem. Rev. 252 (2008) 273–295.
[4] C. Herrero, B. Lassalle-Kaiser, W. Leibl, A.W. Rutherford, A. Aukauloo, Artificial systems related to light driven electron transfer processes in PSII, Coord. Chem. Rev. 252 (2008) 456–468.
[5] H. Dau, I. Zaharieva, Principles, efficiency, and blueprint character of solar-energy conversion in photosynthetic water oxidation, Acc. Chem. Res. 42 (2009) 1861–1870.
[6] A. Magnuson, M. Anderlund, O. Johansson, P. Lindblad, R. Lomoth, T. Polivka, S. Ott, K. Stensjo, S. Styring, V. Sundstrom, L. Hammarstrom, Biomimetic and microbial approaches to solar fuel generation, Acc. Chem. Res. 42 (2009) 1899–1909.
[7] H. Dau, C. Limberg, T. Reier, M. Risch, S. Roggan, P. Strasser, The mechanism of water oxidation: from electrolysis via homogeneous to biological catalysis, ChemCatChem 2 (2010) 724–761.
[8] G.F. Moore, G.W. Brudvig, Energy conversion in photosynthesis: a paradigm for solar fuel production, Annu. Rev. Condens. Matter Phys. 2 (2011) 303–327.
[9] K.N. Ferreira, T.M. Iverson, K. Maghlaoui, J. Barber, S. Iwata, Architecture of the photosynthetic oxygen-evolving center, Science 303 (2004) 1831–1838.
[10] B. Loll, J. Kern, W. Saenger, A. Zouni, J. Biesiadka, Towards complete cofactor arrangement in the 3.0 A resolution structure of photosystem II, Nature 438 (2005) 1040–1044.
[11] H. Dau, A. Grundmeier, P. Loja, M. Haumann, On the structure of the manganese complex of photosystem II: extended-range EXAFS data and specific atomic-resolution models for four S-states, Philos. Trans. R. Soc. London, Ser. B 363 (2008) 1237–1244.
[12] P.E. Siegbahn, A structure-consistent mechanism for dioxygen formation in photosystem II, Chem. Eur. J. 14 (2008) 8290–8302.
[13] Y. Umena, K. Kawakami, J.-R. Shen, N. Kamiya, Crystal structure of oxygen-evolving photosystem II at a resolution of 1.9 Å, Nature 473 (2011) 55–60.
[14] A. Grundmeier, H. Dau, Structural models of the manganese complex of photosystem II and mechanistic implications, Biochim. Biophys. Acta 1817 (2012) 88–105.
[15] H. Dau, M. Haumann, Reaction cycle of photosynthetic water oxidation in plants and cyanobacteria (Response letter), Science 312 (2006) 1471–1472.
[16] H. Dau, M. Haumann, Eight steps preceding O–O bond formation in oxygenic photosynthesis—a basic reaction cycle of the photosystem II manganese complex, Biochim. Biophys. Acta 1767 (2007) 472–483.
[17] E.M. Sproviero, J.A. Gascon, J.P. McEvoy, G.W. Brudvig, V.S. Batista, Quantum mechanics/molecular mechanics study of the catalytic cycle of water splitting in photosystem II, J. Am. Chem. Soc. 130 (2008) 3428–3442.
[18] P.E. Siegbahn, Structures and energetics for O_2 formation in Photosystem II, Acc. Chem. Res. 42 (2009) 1871–1880.
[19] J. Dekker, R. Van Grondelle, Primary charge separation in Photosystem II, Photosynth. Res. 63 (2000) 195–208.
[20] A.R. Holzwarth, M.G. Muller, M. Reus, M. Nowaczyk, J. Sander, M. Rögner, Kinetics and mechanism of electron transfer in intact photosystem II and in the isolated reaction center: pheophytin is the primary electron acceptor, Proc. Nat. Acad. Sci. U.S.A. 103 (2006) 6895–6900.
[21] G. Renger, T. Renger, Photosystem II: the machinery of photosynthetic water splitting, Photosynth. Res. 98 (2008) 53–80.
[22] K. Brettel, E. Schlodder, H.T. Witt, Nanosecond reduction kinetics of photooxidized chlorophyll-alpha-II (P-680) in single flashes as a probe for the electron pathway, H+-release and charge accumulation in the O-2-evolving complex, Biochim. Biophys. Acta 766 (1984) 403–415.
[23] H.J. Eckert, G. Renger, Temperature dependence of P680+ reduction in O2-evolving PS II membrane fragments at different redox states Si of the water oxidizing system, FEBS Lett. 236 (1988) 425–431.
[24] G. Renger, Coupling of electron and proton transfer in oxidative water cleavage in photosynthesis, Biochim. Biophys. Acta 1655 (2004) 195–204.
[25] A.M. Hays, I.R. Vassiliev, J.H. Golbeck, R.J. Debus, Role of D1-His190 in the proton-coupled oxidation of tyrosine YZ in manganese-depleted photosystem II, Biochemistry 38 (1999) 11851–11865.
[26] G. Christen, F. Reifarth, G. Renger, On the origin of the '35-μs kinetics' of P680+· reduction in photosystem II with an intact water oxidising complex, FEBS Lett. 429 (1998) 49–52.
[27] M.J. Schilstra, F. Rappaport, J.H.A. Nugent, C.J. Barnett, D.R. Klug, Proton/hydrogen transfer affects the S-state-dependent microsecond phases of 680+ reduction during water splitting, Biochemistry 37 (1998) 3974–3981.
[28] G. Christen, G. Renger, The role of hydrogen bonds for the multiphasic P680(+)* reduction by YZ in photosystem II with intact oxyen evolution capacity. Analysis of kinetic H/D isotope exchange effects, Biochemistry 38 (1999) 2068–2077.
[29] G. Christen, A. Seeliger, G. Renger, $P680^{+\bullet}$ reduction kinetics and redox transition probability of the water oxidizing complex as a function of pH and H D isotope exchange in spinach thylakoids, Biochemistry 38 (1999) 6082–6092.
[30] C. Jeans, M.J. Schilstra, D.R. Klug, The temperature dependence of P680 + reduction in oxygen-evolving Photosystem II, Biochemistry 41 (2002) 5015–5023.
[31] B. Kok, B. Forbush, M. McGloin, Cooperation of charges in photosynthetic O_2 evolution—I. A linear four-step mechanism, Photochem. Photobiol. 11 (1970) 457–475.
[32] H. Dau, M. Haumann, Time-resolved X-ray spectroscopy leads to an extension of the classical S-state cycle model of photosynthetic oxygen evolution, Photosynth. Res. 92 (2007) 327–343.

[33] A.Y. Mulkidjanian, Photosystem II of green plants: on the possible role of retarded protonic relaxation in water oxidation, Biochim. Biophys. Acta 1410 (1999) 1–6.
[34] M. Karge, K.D. Irrgang, S. Sellin, R. Feinaugle, B. Liu, H.J. Eckert, H.J. Eichler, G. Renger, Effects of hydrogen/deuterium exchange on photosynthetic water cleavage in PS II core complexes from spinach, FEBS Lett. 378 (1996) 140–144.
[35] J.P. Dekker, J.J. Plijter, L. Ouwehand, H.J. van Gorkom, Kinetics of manganese redox transitions in the oxygen evolving apparatus of photosynthesis, Biochim. Biophys. Acta 767 (1984) 176–179.
[36] G. Renger, B. Hanssum, Studies on the reaction coordinates of the water oxidase in PS II membrane fragments from spinach, FEBS Lett. 299 (1992) 28–32.
[37] M. Haumann, P. Liebisch, C. Muller, M. Barra, M. Grabolle, H. Dau, Photosynthetic O_2 formation tracked by time-resolved X-ray experiments, Science 310 (2005) 1019–1021.
[38] C.W. Hoganson, G.T. Babcock, A metalloradical mechanism for the generation of oxygen from water in photosynthesis, Science 277 (1997) 1953–1956.
[39] M. Haumann, W. Junge, Evidence for impaired hydrogen-bonding of tyrosine YZ in calcium-depleted photosystem II, Biochim. Biophys. Acta 1411 (1999) 121–133.
[40] F. Rappaport, J. Lavergne, Coupling of electron and proton transfer in the photosynthetic water oxidase, Biochim. Biophys. Acta 1503 (2001) 246–259.
[41] W. Junge, M. Haumann, R. Ahlbrink, A. Mulkidjanian, J. Clausen, Electrostatics and proton transfer in photosynthetic water oxidation, Philos. Trans. R. Soc. London, Ser. B 357 (2002) 1407–1418.
[42] J. Lavergne, W. Junge, Proton release during the redox cycle of the water oxidase, Photosynth. Res. 38 (1993) 279–296.
[43] M. Haumann, W. Junge, in: D. Ort, C.F. Yocum (Eds.), Oxygenic Photosynthesis: The Light Reactions, Kluwer Academic Publ., Dordrecht, 1996, pp. 165–192.
[44] E. Schlodder, H.T. Witt, Stoichiometry of proton release from the catalytic center in photosynthetic water oxidation. Reexamination by a glass electrode study at ph 5.5–7.2, J. Biol. Chem. 274 (1999) 30387–30392.
[45] H. Suzuki, M. Sugiura, T. Noguchi, Monitoring proton release during photosynthetic water oxidation in photosystem II by means of isotope-edited infrared spectroscopy, J. Am. Chem. Soc. 131 (2009) 7849–7857.
[46] S.E. Braslavsky, Photoacoustic and photothermal methods applied to the study of radiationless deactivation processes in biological systems and in substances of biological interest, Photochem. Photobiol. 43 (1986) 667–675.
[47] S.E. Braslavsky, G.E. Heibel, Time-resolved photothermal and photoacoustic methods applied to photoinduced processes in solution, Chem. Rev. 92 (1992) 1381–1410.
[48] T. Gensch, C. Viappiani, Time-resolved photothermal methods: accessing time-resolved thermodynamics of photoinduced processes in chemistry and biology, Photochem. Photobiol. Sci. 2 (2003) 699–721.
[49] R. Delosme, On some aspects of photosynthesis revealed by photoacoustic studies: a critical evaluation, Photosynth. Res. 76 (2003) 289–301.
[50] H.J.M. Hou, D. Mauzerall, Listening to PS II: enthalpy, entropy, and volume changes, J. Photochem. Photobiol., B 104 (2011) 357–365.
[51] J.B. Callis, W.W. Parson, M. Gouterman, Fast changes of enthalpy and volume on flash excitation of chromatium chromatophores, Biochim. Biophys. Acta 267 (1972) 348–362.
[52] H. Arata, W.W. Parson, Enthalpy and volume changes accompanying electron transfer from P-870 to quinones in *Rhodopseudomonas sphaeroides* reaction centers, Biochim. Biophys. Acta 636 (1981) 70–81.
[53] P. Poulet, D. Cahen, S. Malkin, Photo-acoustic detection of photosynthetic oxygen evolution from leaves—quantitative-analysis by phase and amplitude measurements, Biochim. Biophys. Acta 724 (1983) 433–446.
[54] O. Canaani, S. Malkin, D. Mauzerall, Pulsed photoacoustic detection of flash-induced oxygen evolution from intact leaves and its oscillations, Proc. Nat. Acad. Sci. U.S.A. 85 (1988) 4725–4729.
[55] H. Dau, U.P. Hansen, Studies on the adaptation of intact leaves to changing light intensities by a kinetic analysis of chlorophyll fluorescence and oxygen evolution as measured by the photoacoustic signal, Photosynth. Res. 20 (1989) 59–83.
[56] H. Dau, U.P. Hansen, A study on the energy-dependent quenching of chlorophyll fluorescence by means of photoacoustic measurements, Photosynth. Res. 25 (1990) 269–278.
[57] J.M. Hou, V.A. Boichenko, B.A. Diner, D. Mauzerall, Thermodynamics of electron transfer in oxygenic photosynthetic reaction centers: volume change, enthalpy, and entropy of electron-transfer reactions in manganese-depleted photosystem II core complexes, Biochemistry 40 (2001) 7117–7125.
[58] V.A. Boichenko, J.M. Hou, D. Mauzerall, Thermodynamics of electron transfer in oxygenic photosynthetic reaction centers: volume change, enthalpy, and entropy of electron-transfer reactions in the intact cells of the cyanobacterium Synechocystis PCC 6803, Biochemistry 40 (2001) 7126–7132.
[59] H. Conjeaud, P. Mathis, The effects of pH on the reductions kinetics of P-680 in Tris-treated chloroplasts, Biochim. Biophys. Acta 590 (1980) 353–359.
[60] R. Ahlbrink, M. Haumann, D. Cherepanov, O. Boegershausen, A. Mulkidjanian, W. Junge, Function of tyrosine-Z in water oxidation by photosystem II: electrostatical promotor instead of hydrogen abstractor, Biochemistry 37 (1998) 1131–1142.
[61] H.J.M. Hou, D. Mauzerall, The A-FX to FA/B step in synechocystis 6803 photosystem I is entropy driven, J. Am. Chem. Soc. 128 (2006) 1580–1586.
[62] A. Losi, I. Yruela, M. Reus, A.R. Holzwarth, S.E. Braslavsky, Structural changes upon excitation of D1–D2-Cyt b559 photosystem II reaction centers depend on the beta-carotene content, Photochem. Photobiol. Sci. 2 (2003) 722–729.
[63] L. Iuzzolino, J. Dittmer, W. Dörner, W. Meyer-Klaucke, H. Dau, X-ray absorption spectroscopy on layered photosystem II membrane particles suggests manganese-centered oxidation of the oxygen-evolving complex for the S_0–S_1, S_1–S_2, and S_2–S_3 transitions of the water oxidation cycle, Biochemistry 37 (1998) 17112–17119.
[64] H. Schiller, H. Dau, Preparation protocols for high-activity photosystem II membrane particles of green algae and higher plants, pH dependence of oxygen evolution and comparison of the S_2-state multiline signal by X-band EPR spectroscopy, J. Photochem. Photobiol., B 55 (2000) 138–144.
[65] D.A. Berthold, G.T. Babcock, C.F. Yocum, A highly resolved, oxygen-evolving photosystem-II preparation from spinach thylakoid membranes—electron-paramagnetic-Res and electron-transport properties, FEBS Lett. 134 (1981) 231–234.
[66] T. Autrey, A new angle into time-resolved photoacoustic spectroscopy: a layered prism cell increases experimental flexibility, Rev. Sci. Instrum. 69 (1998) 2246.
[67] A. Guskov, J. Kern, A. Gabdulkhakov, M. Broser, A. Zouni, W. Saenger, Cyanobacterial photosystem II at 2.9-Å resolution and the role of quinones, lipids, channels and chloride, Nat. Struct. Mol. Biol. 16 (2009) 334–342.
[68] R. Krivanek, J. Kern, A. Zouni, H. Dau, M. Haumann, Spare quinones in the Q_B cavity of crystallized photosystem II from *Thermosynechococcus elongatus*, Biochim. Biophys. Acta 1767 (2007) 520–527.
[69] L. Gerencser, H. Dau, Water oxidation by photosystem II: H2O–D2O exchange and the influence of pH support formation of an intermediate by removal of a proton before dioxygen creation, Biochemistry 49 (2010) 10098–10106.
[70] J.R. Small, L.J. Libertini, E.W. Small, Analysis of photoacoustic waveforms using the nonlinear least squares method, Biophys. Chem. 42 (1992) 29–48.
[71] G.J. Edens, M.R. Gunner, Q. Xu, D. Mauzerall, The enthalpy and entropy of reaction for formation of P+QA− from excited reaction centers of *Rhodobacter sphaeroides*, J. Am. Chem. Soc. 122 (2000) 1479–1485.
[72] R.C. Weast, 51st ed. The Chemical Rubber Co, Ohio, 1970.
[73] J.-L.H. Jiwan, A.K. Chibisov, S.E. Braslavsky, Volume changes associated with electron transfer quenching of excited Ru(bpy)32+ and xanthene dyes. Time-resolved optoacoustic studies, J. Phys. Chem. 99 (1995) 10246–10250.
[74] A. Losi, S.E. Braslavsky, W. Gärtner, J.L. Spudich, Time-Resolved Absorption and Photothermal Measurements with Sensory Rhodopsin I from Halobacterium salinarum, Biophys. J. 76 (1999) 2183–2191.
[75] Y.L. Shek, T.V. Chalikian, Volumetric characterization of interactions of glycine betaine with protein groups, J. Phys. Chem. B 115 (2011) 11481–11489.
[76] J. Messinger, W.P. Schroder, G. Renger, Structure-function relations in photosystem II. Effects of temperature and chaotropic agents on the period four oscillation of flash-induced oxygen evolution, Biochemistry 32 (1993) 7658–7668.
[77] M. Grabolle, H. Dau, Efficiency and role of loss processes in light-driven water oxidation by PSII, Physiol. Plant. 131 (2007) 50–63.
[78] H.J. Eckert, N. Wiese, J. Bernarding, H.J. Eichler, G. Renger, Analysis of the electron transfer from Pheo- to QA in PS II membrane fragments from spinach by time resolved 325 nm absorption changes in the picosecond domain, FEBS Lett. 240 (1988) 153–158.
[79] R. Delosme, D. Beal, P. Joliot, Photoacoustic detection of flash-induced charge separation in photosynthetic systems—spectral dependence of the quantum yield, Biochim. Biophys. Acta 1185 (1994) 56–64.
[80] M. Grabolle, Die Donorseite des Photosystems II: Rekombinationsfluoreszenz- und Röntgenabsorptionsstudien (thesis), Fachbereich Physik, Freie Univ. Berlin, http://www.diss.fu-berlin.de/2005/174/ (2005).
[81] R. Emerson, M.L. Charlton, The dependence of the quantum yield of chlorella photosynthesis on wave length of light, Am. J. Bot. 30 (1943) 165–178.
[82] R. Emerson, The quantum yield of photosynthesis, Annu. Rev. Plant Physiol. 9 (1958) 1–24.
[83] D. Mauzerall, J.M. Hou, V.A. Boichenko, Volume changes and electrostriction in the primary photoreactions of various photosynthetic systems: estimation of dielectric coefficient in bacterial reaction centers and of the observed volume changes with the Drude–Nernst equation, Photosynth. Res. 74 (2002) 173–180.
[84] K. Takeshita, N. Hirota, Y. Imamoto, M. Kataoka, F. Tokunaga, M. Terazima, Temperature-dependent volume change of the initial step of the photoreaction of photoactive yellow protein (PYP) studied by transient grating, J. Am. Chem. Soc. 122 (2000) 8524–8528.
[85] B. Meyer, E. Schlodder, J.P. Dekker, H.T. Witt, O2 evolution and Chl a+II (P-680+) nanosecond reduction kinetics in single flashes as a function of pH, Biochim. Biophys. Acta 974 (1989) 36–43.
[86] J. Feitelson, D. Mauzerall, Enthalpy and electrostriction in the electron-transfer reaction between triplet zinc uroporphyrin and ferricyanide, J. Phys. Chem. B 106 (2002) 9674–9678.
[87] A.C. Rizzi, M. van Gastel, P.A. Liddell, R.E. Palacios, G.F. Moore, G. Kodis, A.L. Moore, T.A. Moore, D. Gust, S.E. Braslavsky, Entropic changes control the charge separation process in triads mimicking photosynthetic charge separation, J. Phys. Chem. A 112 (2008) 4215–4223.
[88] P. Drude, W. Nernst, Über Elektrostriktion durch freie Ionen, Z. Phys. Chem. 15 (1894) 79–85.
[89] C.D. Borsarelli, H. Corti, D. Goldfarb, S.E. Braslavsky, Structural volume changes in photoinduced electron transfer reactions. Laser-induced optoacoustic studies of speciation during the quenching reaction of excited Ru(bpy)32+ by Fe(III) in aqueous solutions, J. Phys. Chem. A 101 (1997) 7718–7724.
[90] C.D. Borsarelli, S.E. Braslavsky, Enthalpy, volume, and entropy changes associated with the electron transfer reaction between the 3MLCT state of Ru(Bpy)32+ and methyl viologen cation in aqueous solutions, J. Phys. Chem. A 103 (1999) 1719–1727.
[91] H.T. Witt, Primary reactions of oxygenic photosynthesis, Ber. Bunsenges. Phys. Chem. 100 (1996) 1923–1942.
[92] F. Rappaport, M. Guergova-Kuras, P.J. Nixon, B.A. Diner, J. Lavergne, Kinetics and pathways of charge recombination in Photosystem II, Biochemistry 41 (2002) 8518–8527.
[93] F. Rappaport, A. Cuni, L. Xiong, R. Sayre, J. Lavergne, Charge recombination and thermoluminescence in photosystem II, Biophys. J. 88 (2005) 1948–1958.

[94] K. Cser, I. Vass, Radiative and non-radiative charge recombination pathways in Photosystem II studied by thermoluminescence and chlorophyll fluorescence in the cyanobacterium Synechocystis 6803, Biochim. Biophys. Acta 1767 (2007) 233–243.
[95] I. Vass, Role of charge recombination processes in photodamage and photoprotection of the photosystem II complex, Physiol. Plant. 142 (2011) 6–16.
[96] I. Zaharieva, J.M. Wichmann, H. Dau, Thermodynamic limitations of photosynthetic water oxidation at high proton concentrations, J. Biol. Chem. 286 (2011) 18222–18228.
[97] H. Dau, L. Iuzzolino, J. Dittmer, The tetra-manganese complex of photosystem II during its redox cycle: X-ray absorption results and mechanistic implications, Biochim. Biophys. Acta 1503 (2001) 24–39.
[98] H. Dau, P. Liebisch, M. Haumann, X-ray absorption spectroscopy to analyze nuclear geometry and electronic structure of biological metal centers—potential and questions examined with special focus on the tetra-nuclear manganese complex of oxygenic photosynthesis, Anal. Bioanal. Chem. 376 (2003) 562–583.
[99] J.H. Robblee, R.M. Cinco, V.K. Yachandra, X-ray spectroscopy-based structure of the Mn cluster and mechanism of photosynthetic oxygen evolution, Biochim. Biophys. Acta 1503 (2001) 7–23.
[100] D.A. Pantazis, M. Orio, T. Petrenko, S. Zein, W. Lubitz, J. Messinger, F. Neese, Structure of the oxygen-evolving complex of photosystem II: information on the S_2 state through quantum chemical calculation of its magnetic properties, Phys. Chem. Chem. Phys. 11 (2009) 6788–6798.
[101] S. Schinzel, J. Schraut, A.V. Arbuznikov, P.E.M. Siegbahn, M. Kaupp, Density functional calculations of ^{55}Mn, ^{14}N and ^{13}C electron paramagnetic resonance parameters support an energetically feasible model system for the S_2 state of the oxygen-evolving complex of photosystem II, Chem. Eur. J. 16 (2010) 10424–10438.